Research Square

Preprints are preliminary reports that have not undergone peer review.
They should not be considered conclusive, used to inform clinical practice,
or referenced by the media as validated information.

Fault growth, displacement scaling and segment interaction in a gravity-driven Niger Delta fault network: Insights from 3D seismic data

T. Omeru[1]
University of Lagos
O. Adegbemiro
tadegbemiro@gmail.com
University of Lagos
A. Opatola
University of Lagos

Research Article

Keywords: Niger Delta, growth faults, fault interaction, displacement-length scaling, relay ramps, reservoir compartmentalization

Posted Date: November 11th, 2026

DOI: https://doi.org/10.21203/rs.3.rs-11479296/v1

License: This work is licensed under a Creative Commons Attribution 4.0 International License.
Read Full License

Additional Declarations: No competing interests reported.

Fault growth, displacement scaling and segment interaction in a gravity-driven Niger Delta fault network: Insights from 3D seismic data

T. Omeru[1], O. Adegbemiro[2]*, A. Opatola[3]

[1,2,3] Department of Geoscience, University of Lagos, Lagos, Nigeria

*Correspondence: tadegbemiro@gmail.com

ABSTRACT

Growth-fault systems in deltaic basins evolve through propagation, interaction and possible linkage, but these processes are difficult to distinguish from geometry alone. This study integrates 3D seismic interpretation and wireline-log correlation to investigate fault growth and segment interaction in the TOYO Field, Niger Delta.

Sixty-four faults were mapped across four Agbada Formation horizons (A, B, F and I); 18 faults were selected for quantitative analysis. Analyses included along-strike throw-distance (T-X) and throw-depth (T-Z) profiles, displacement-length (D-L) scaling, relay geometry, and structural maps.

Fault lengths range from 0.42 to 19.0 km, defining E-W, NE-SW and NW-SE groups. Kruskal-Wallis tests found no differences among these groups in fault length ($p = 0.0554$) or maximum throw ($p = 0.7251$). T-X profiles range from symmetrical and flat-topped to asymmetric, double-peaked and irregular. Faults with complex profiles were longer than those with simple profiles (median 4.27 versus 1.77 km; Mann-Whitney $U = 6.0$, $p = 0.0019$), whereas maximum throw did not differ ($p = 0.2463$). This association may partly reflect greater measurement density on longer faults.

Four candidate relay relationships and four candidate interaction/linkage relationships were identified; relay overlap/separation ratios range from 2.48 to 9.65. The geometries and displacement patterns are consistent with segment interaction, displacement redistribution, relay development and possible linkage, but do not establish an evolutionary sequence or prove hard linkage. The analysis provides a framework for evaluating reservoir compartment geometry, although fault sealing and hydraulic connectivity cannot be inferred from geometry alone.

.

Keywords: *Niger Delta; growth faults; fault interaction; displacement-length scaling; relay ramps; reservoir compartmentalization.*

Statements and Declarations

Funding

The authors received no specific funding for this research.

Competing Interests

The authors declare that they have no financial or non-financial competing interests that are directly or indirectly related to this work.

Author Contributions

T. Omeru contributed to conceptualization, supervision, and critical review of the manuscript. O. Adegbemiro contributed to data curation, seismic interpretation, methodology, formal analysis, visualization, and original manuscript preparation. A. Opatola contributed to geological interpretation, validation of results, and critical review and editing of the manuscript. All authors read and approved the final manuscript.

Data Availability

The data supporting the findings of this study were derived from 3D seismic and wireline-log datasets from the TOYO Field, Niger Delta, Nigeria. Access to the underlying datasets may be subject to confidentiality or licensing restrictions. Data availability is therefore subject to the relevant data-owner permissions. Further information may be requested from the corresponding author, subject to these restrictions.

1. Introduction

Normal faults within the Niger Delta growth-fault system exert a first-order control on sediment accommodation, structural trap development and reservoir compartmentalization in deltaic basins. In the Niger Delta, gravitational deformation of the prograding sedimentary wedge above weak, overpressured Akata Formation shale has generated extensive syn-depositional normal-fault systems within the paralic Agbada Formation (Evamy et al. 1978; Doust and Omatsola 1990; Tuttle et al. 1999; Corredor et al. 2005). These structures range from relatively simple fault segments to kilometre-scale fault arrays and are fundamental components of the structural architecture of many Niger Delta hydrocarbon fields.

The present-day geometry of a normal fault does not necessarily record a simple history of continuous propagation. Normal faults may initiate as discrete segments, propagate laterally and vertically, enter the stress fields of neighbouring structures, interact across overlap zones and, in some cases, become structurally linked into larger composite faults (Peacock and Sanderson 1991; Childs et al. 1995; Crider and Pollard 1998; Peacock 2002; Walsh et al. 2003; Childs et al. 2017). Relay zones are particularly important because they can accommodate displacement transfer between overlapping fault segments, while progressive interaction and relay breaching may produce increasingly complex fault geometries and displacement distributions (Peacock and Sanderson 1991, 1994; Childs et al. 1995; Imber et al. 2004).

This behaviour provides a useful conceptual fault-growth spectrum:

isolated fault growth, lateral and vertical segment propagation, segment interaction and relay development, relay breaching and possible linkage, displacement redistribution.

Individual stages, however, cannot necessarily be diagnosed from a single geometric parameter. Relatively simple displacement-distance profiles may be compatible with comparatively uncomplicated fault growth, whereas interaction and linkage can generate asymmetric or multi-peaked displacement distributions and displacement minima associated with segment boundaries or linkage zones (Peacock and Sanderson 1991; Bürgmann et al. 1994; Childs et al. 1995; Nicol et al. 1996; Willemse et al. 1996). Such geometries are not, by themselves, proof of linkage because displacement patterns may also be influenced by structural inheritance, stratigraphic heterogeneity, measurement uncertainty and incomplete seismic imaging. Similarly, geometrical overlap indicates that neighbouring faults are positioned to interact, but overlap alone does not demonstrate physical linkage (Childs et al. 1995; Crider and Pollard 1998; Imber et al. 2004; Walsh et al. 2003).

Displacement-length (D-L) relationships provide an additional quantitative framework for evaluating fault populations. Maximum displacement commonly increases with fault length and is conventionally represented by a power-law relationship of the form $D_{max} = cL^n$ (Walsh and Watterson 1988; Cowie and Scholz 1992; Dawers et al. 1993; Scholz et al. 1993; Kim and Sanderson 2005). However, substantial scatter is common in natural fault populations, and D-L relationships may be influenced by fault type, segmentation and linkage, reactivation,

mechanical properties, measurement method and the resolution of low-displacement fault tips (Cartwright et al. 1995; Kim and Sanderson 2005; Torabi and Berg 2011). Consequently, present-day D-L scaling provides useful information about fault populations but should not, by itself, be interpreted as a unique record of fault-growth history (Walsh et al. 2002; Kim and Sanderson 2005; Rotevatn et al. 2019).

These considerations are particularly relevant to the Niger Delta, where rapid sedimentation, differential loading, gravitational extension and deformation above weak Akata Formation shale have produced structurally complex syn-sedimentary fault systems (Doust and Omatsola 1990; Tuttle et al. 1999; Corredor et al. 2005). Three-dimensional seismic studies have documented segmentation, relay development, displacement variability and fault interaction within Niger Delta normal-fault systems (Fazli Khani and Back 2012; Fazlikhani and Back 2015; Fazlikhani et al. 2017; Umar et al. 2019). Umar et al. (2019), for example, documented isolated and coherently linked normal faults, relay ramps and variable throw distributions in an onshore Niger Delta field. Fazlikhani and Back (2015) demonstrated that initially separate segments of a syn-sedimentary Niger Delta fault system underwent lateral propagation and linkage to form an approximately 15-km-long master fault while retaining characteristics inherited from the earlier segmented geometry.

The TOYO Field, located within the Coastal Swamp Depobelt of the eastern Niger Delta, provides an opportunity to examine these relationships within a densely faulted 3D seismic dataset. The field contains a fault network intersecting four correlated Agbada Formation horizons and is constrained by five wells and 3D seismic data. Although seismic interpretation establishes the structural framework, the relationships among fault size, orientation, displacement distribution, segmentation, relay geometry and stratigraphic thickness require integrated quantitative analysis. The present study therefore evaluates these attributes collectively rather than relying on any single geometric criterion to infer fault-growth state.

The novelty of this study lies not in documenting relay structures or fault linkage in the Niger Delta per se, but in testing whether multiple complementary geometric and displacement attributes within a single fault population provide mutually consistent evidence for progressive fault interaction. By integrating along-strike and vertical displacement distributions, displacement-length scaling, relay geometry, orientation statistics and stratigraphic thickness variations, the study evaluates whether increasingly complex fault geometries can be distinguished from simple orientation-controlled fault growth. This provides a quantitative framework for relating fault-network evolution to structural reservoir compartment geometry in a gravity-driven deltaic setting.

We test the hypothesis that progressive interaction within the TOYO fault network should be expressed by a transition from relatively simple displacement profiles toward increasingly asymmetric, multi-peaked and irregular displacement distributions associated spatially with overlapping relay and candidate linkage geometries.

Accordingly, this study addresses the following question:

To what extent do fault geometry, displacement distributions, relay relationships and candidate interaction/linkage geometries record progressive fault interaction within a gravity-driven Niger Delta fault network, and what are the implications for structural reservoir compartmentalization?

The study therefore aims to: (1) characterize fault geometry and orientation; (2) evaluate along-strike and vertical displacement variability; (3) quantify displacement-length relationships; (4) examine geometric and displacement evidence for fault interaction and relay development; and (5) integrate these observations with stratigraphic thickness and structural maps to develop a constrained conceptual model of fault-network evolution and reservoir compartment geometry.

2. Geological Setting

The TOYO Field is located approximately 32 km southeast of Port Harcourt within the Coastal Swamp Depobelt of the eastern Niger Delta, Rivers State, Nigeria. The Niger Delta consists broadly of the Akata, Agbada and Benin stratigraphic units, representing a major regressive clastic succession developed during progressive delta progradation (Evamy et al. 1978; Doust and Omatsola 1990). The four stratigraphic intervals examined in this study A, B, F and I, listed in order of increasing depth occur within the paralic Agbada Formation and were correlated across five wells using gamma-ray and deep-resistivity logs.

The structural style of the Niger Delta reflects gravitational deformation of the prograding sedimentary wedge above weak, overpressured marine shale of the Akata Formation. Differential sediment loading and downslope translation generated extensive syn-sedimentary normal faulting in the extensional domain, while deformation farther basinward includes contractional structures above weak Akata detachments (Doust and Omatsola 1990; Tuttle et al. 1999; Corredor et al. 2005). Within the extensional domain, growth faults, antithetic structures and associated rollover geometries strongly influence accommodation and structural compartment geometry (Fazli Khani and Back 2012; Fazlikhani et al. 2017).

For the present study, regional shale mobility is treated as the tectonic framework rather than as a locally demonstrated mechanism. The available TOYO dataset does not independently establish local Akata shale mobilization beneath individual faults**.**

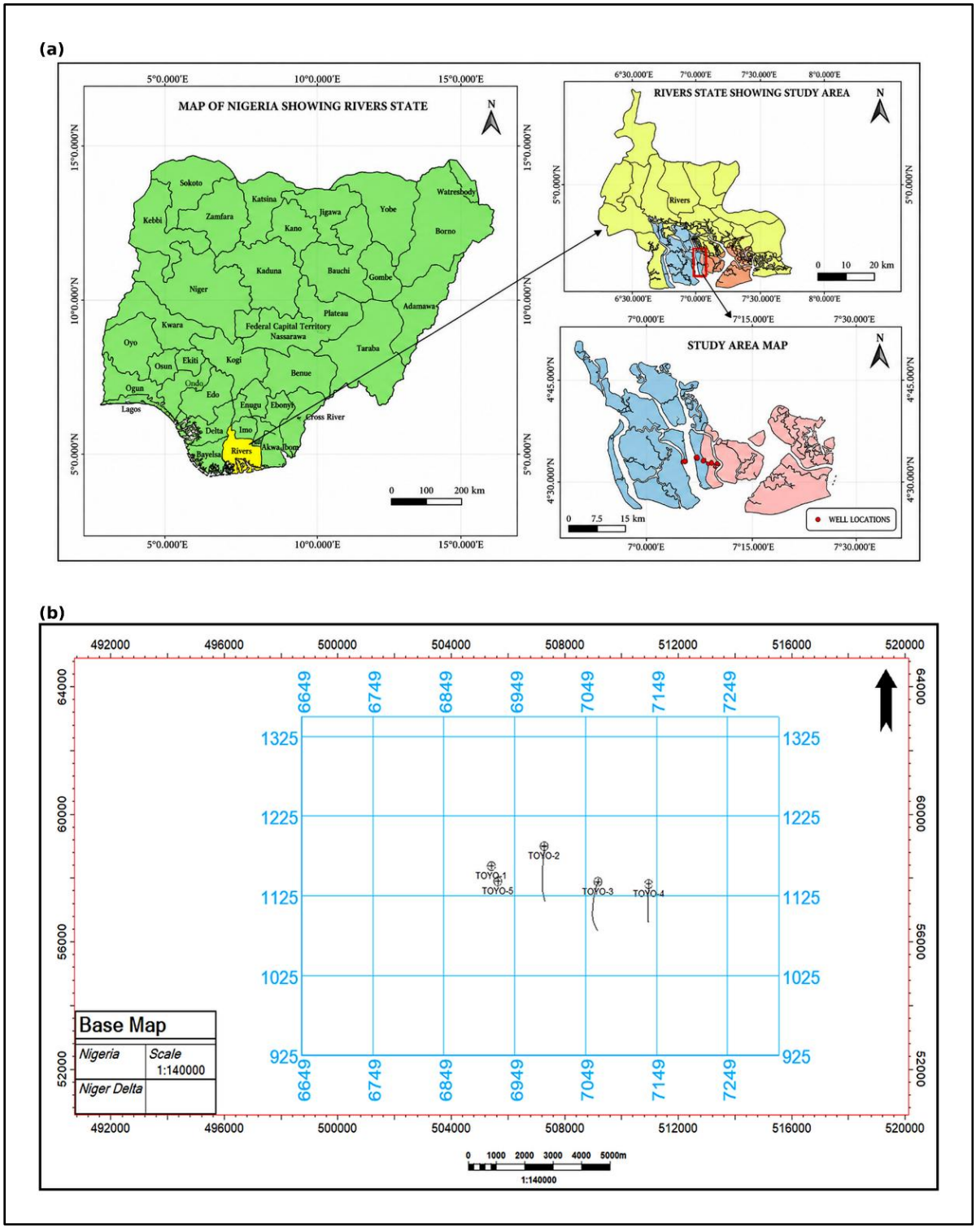


Fig. 1: Location and geological setting of the TOYO Field within the Coastal Swamp Depobelt of the Niger Delta, Nigeria. (a) Regional location of the study area in Rivers State; (b) TOYO Field base map showing the locations of wells TOYO-01 to TOYO-05 within the 3D seismic survey area.

3. Data and Methods

3.1 Well correlation and seismic interpretation

Wireline data from TOYO-01 to TOYO-05 were quality controlled and integrated with the 3D seismic volume in Petrel. Gamma-ray and deep-resistivity logs were used to correlate four sand-prone stratigraphic intervals designated A, B, F and I. Checkshot data provided time-depth control for seismic-well correlation. The four corresponding reflectors were interpreted throughout the seismic volume and used to generate time and depth structure surfaces.

Faults were recognized from reflector discontinuities, offsets and characteristic fault related geometries. Fault sticks interpreted on seismic sections were correlated to construct three-dimensional fault surfaces.

Sixty-four faults were initially mapped. Eighteen principal faults were selected for quantitative analysis because they could be traced across sufficient seismic coverage and provided fault-length and displacement measurements with acceptable confidence. This selection introduces an unavoidable bias toward larger and more seismically resolvable structures and may underrepresent short or low-displacement faults. The 18-fault subset was used consistently for the comparative fault-geometry and displacement-profile analyses. Horizon-specific displacement-length measurements were evaluated separately, with one observation per selected fault at each interpreted horizon.

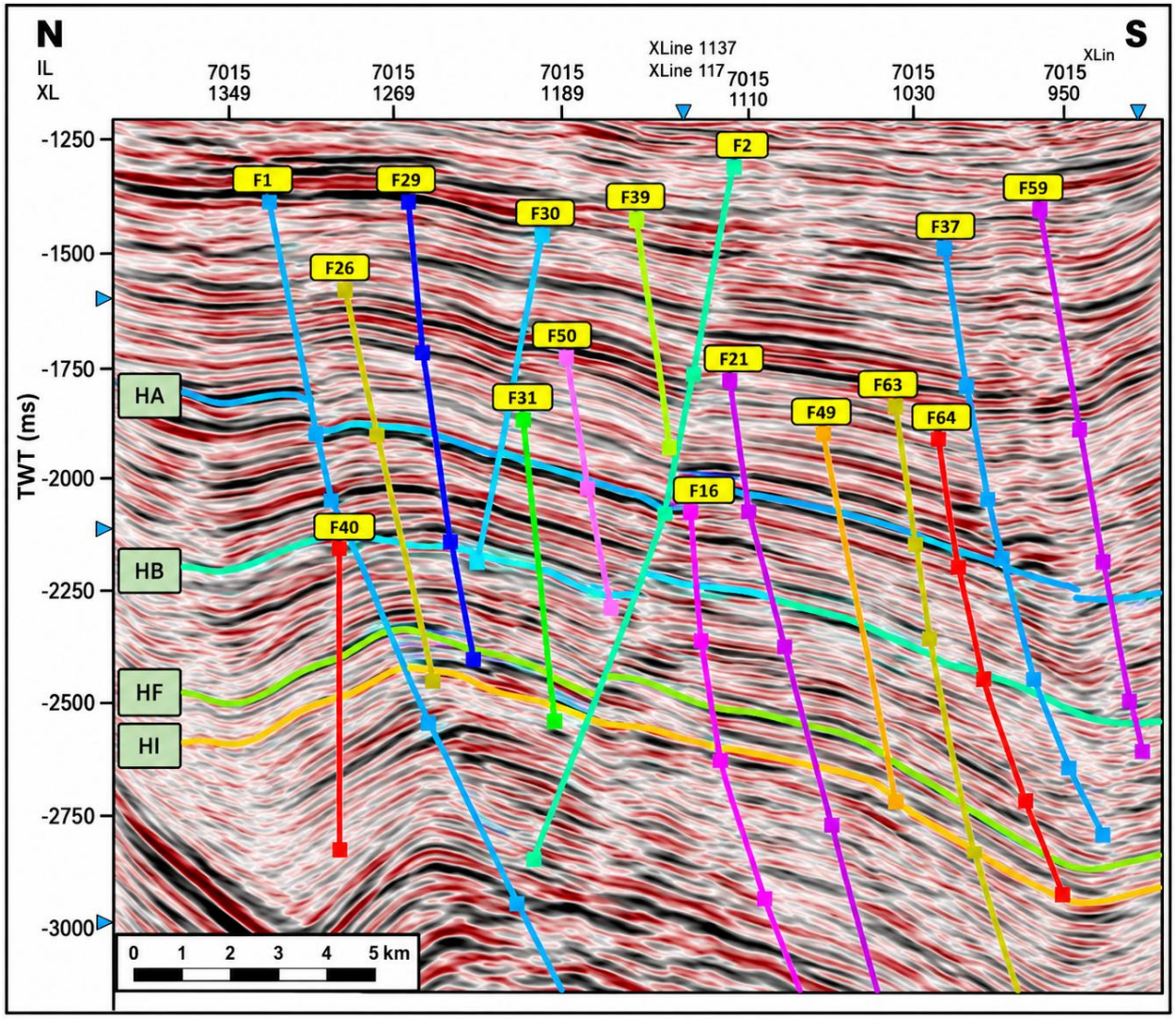


Fig. 2: Representative seismic section through the TOYO Field showing the interpreted Horizons A, B, F and I and the principal normal faults used to define the structural framework

3.2 Fault geometry and orientation

Fault-trace orientation, dip direction, fault length and throw were extracted from the interpreted 3D fault models. Fault orientations were standardized as axial data in the 0-180° range and displayed using rose diagrams with a 10° bin interval. Based on the observed orientation distribution, the 18 principal faults were grouped into E-W, NE-SW and NW-SE populations. Because group sizes were small and unequal, fault length and maximum throw were compared among the three orientation groups using separate Kruskal-Wallis tests at $\alpha = 0.05$.

Fault dip azimuths were calculated from the measured fault-strike orientations and independently interpreted dip polarity. The two possible dip azimuths for each fault were determined perpendicular to strike, and the appropriate

azimuth was selected based on whether the fault dipped broadly northward or southward. The resulting dip azimuths range from 5° to 250°, with 13 faults dipping broadly southward and five dipping broadly northward. These values represent geometrically derived dip directions rather than independently measured three-dimensional fault-plane orientations.

3.3 Along-strike displacement analysis

Throw was measured at multiple positions between the interpreted tips of each fault using seismic sections selected approximately perpendicular to fault strike. Cumulative along-strike distance was calculated from successive X-Y measurement coordinates referenced to the interpreted fault trace. Because fault lengths vary substantially, differences in measurement spacing and sampling density may affect the identification of throw maxima, minima and profile irregularities. Additional uncertainty arises from seismic resolution and fault-tip interpretation. Consequently, local throw fluctuations were not automatically interpreted as separate fault segments unless supported by the mapped fault geometry.

Throw-distance (T-X) profiles were classified as symmetrical, asymmetric, double-peaked, flat-topped or irregular/complex. These profiles were compared with mapped fault geometry and neighbouring faults to identify displacement patterns potentially associated with segmentation and interaction.

Profile geometry was not treated as independent proof of propagation direction or linkage.

3.4 Statistical analysis of displacement-profile complexity

To evaluate whether fault size is associated with along-strike displacement-profile complexity, the five identified T-X profile types were consolidated into two broader categories. Symmetrical and flat-topped profiles were classified as relatively simple because they exhibit comparatively regular displacement distributions, whereas asymmetric, double-peaked and irregular profiles were classified as complex because they display pronounced displacement asymmetry, multiple displacement maxima or irregular along-strike variations. This classification was based on the observed profile geometry rather than an assumed fault-growth stage. The simple and complex categories contained seven and eleven faults, respectively. Although the classification provides a consistent framework for statistical comparison, the interpretation of profile complexity remains partly dependent on the spatial resolution and sampling density of the displacement measurements.

Fault size was represented by the maximum mapped fault length across Horizons A, B, F and I, while displacement magnitude was represented by the maximum throw recorded across the four horizons. Differences in fault length and maximum throw between the simple and complex profile groups were evaluated using two-sided Mann-Whitney U tests with exact p-values and no continuity correction. Separate Kruskal-Wallis tests were used to compare fault length and maximum throw among the three orientation groups. Rank-biserial correlation was calculated as an effect-size measure for the Mann-Whitney comparisons, and statistical significance was assessed at $\alpha = 0.05$.

The simple-complex classification was treated as an operational measure of along-strike displacement-profile geometry rather than a direct indicator of fault-growth stage. The statistical comparisons were therefore interpreted as tests of association, recognizing that profile complexity may also be influenced by fault length, sampling density, stratigraphic variability and seismic resolution.

3.5 Throw-depth analysis

Throw was measured at Horizons A, B, F and I and plotted against depth. Five T-Z patterns were recognized: expanding, non-monotonic, blocky, restricted-to-depth and waning-with-depth.

Because only four stratigraphic levels were available, these profiles characterize vertical displacement variability but cannot uniquely reconstruct the timing of fault initiation, reactivation or propagation.

3.6 Displacement-length scaling

Displacement-length (D-L) scaling relationships were evaluated for 18 principal faults across four interpreted seismic horizons (A, B, F and I). Fault length (L) and maximum displacement (D_{max}) were expressed in metres and used to evaluate the scaling relationship. Maximum throw, which was measured separately in feet, was not substituted for maximum displacement in the D-L analysis. The relationship between fault length and maximum displacement was expressed using the power-law equation:

$$D_{max} = cL^{n}$$

where D_{max} is maximum displacement, L is fault length, c is the scaling coefficient and n is the scaling exponent. The relationship was linearized as:

$$\mathrm{Log}_{10}(D_{max}) = \log_{10}(c) + n \log_{10}(L)$$

Ordinary least-squares linear regression was performed independently for each horizon using logarithmically transformed measurements. Regression slopes, intercepts, coefficients of determination (R^2), p-values and 95% confidence intervals were obtained to assess the scaling relationships.

3.7 Relay and interaction/linkage geometry

Eight structurally significant fault relationships were examined from the fault-polygon and depth-structure maps and subdivided into four candidate relay relationships: R1 (F17-F42), R2 (F42-F13), R3 (F23-F55) and R4 (F3-F5); and four candidate interaction/linkage relationships: L1 (F1-F17), L2 (F2-F13), L3 (F2-F16) and L4 (F21-F49). For the relay candidates, overlap (O) was measured parallel to the general fault trend and separation (S) perpendicular to it. The overlap/separation ratio (O/S) was calculated as a descriptive measure of relay geometry.

The interaction/linkage candidates were identified from converging, connected or near-continuous map-view fault geometries and were evaluated together with the corresponding displacement patterns and structural continuity. O/S ratios were not used to establish hard linkage, and candidate linkage was distinguished from demonstrated hard linkage unless a continuous connecting fault surface could be resolved from the seismic interpretation.

The overlap/separation ratio was calculated as:

$$R_{OS} = \frac{O}{S}$$

where R_{OS} is the dimensionless overlap/separation ratio, (O) represents the along-strike overlap between adjacent fault segments (m), and (S) represents their perpendicular separation (m). Higher R_{OS} values indicate greater geometrical overlap relative to fault separation but do not independently demonstrate displacement transfer or physical linkage.

3.8 Isochore and compartment analysis

Isochore maps were examined for spatial changes in interval thickness and compared with fault geometry and T-Z behaviour. Thickness patterns were considered possible indicators of differential accommodation, loading and syn-sedimentary deformation rather than direct proof of shale mobilization.

Finally, fault geometry, relay relationships and displacement distributions were integrated to identify structurally distinct fault-bounded domains. No fault-seal calculation was performed; therefore, the analysis predicts structural compartment geometry rather than hydraulic compartmentalization.

4. Results

4.1 Fault geometry and orientation

The 18 principal faults display considerable variation in length and throw. Across the four mapped horizons, fault lengths range from approximately 0.42 km for F13 to 19.0 km for F2. Maximum observed throws range from <100 ft on the smallest structures to >700 ft on F2.

Seven faults belong to the E-W family, four to the NE-SW family and seven to the NW-SE family. Thirteen faults dip south, southwest or southeast and are broadly basinward-directed. Five dip northward or northeastward; four of these F12, F13, F17 and F42 form a spatially concentrated northwestern antithetic cluster.

The E-W population has a mean length of 7,626 m compared with 4,270 m for NE-SW and 2,479 m for NW-SE faults. Although descriptive differences in fault length occur among the three orientation groups, the Kruskal-Wallis test does not identify a statistically significant difference at the 0.05 significance level ($H(2) = 5.786$, $p = 0.0554$). Similarly, maximum throw does not differ significantly among the orientation groups ($H(2) = 0.643$, $p = 0.7251$). These findings suggest that fault orientation alone is insufficient to explain the observed variation in fault dimensions within the analyzed population. However, the relatively small and unequal group sizes limit the statistical power of the comparisons, and an influence of fault orientation cannot be excluded.

Table 1: Geometric characteristics, fault orientations, maximum mapped lengths, maximum throws, along-strike displacement-profile classifications and sampling counts for the 18 principal faults interpreted in the TOYO Field.

Fault ID	Strike (°)	Orientation group	Dip azimuth (°)	Maximum length (m)	Maximum throw (ft)	T-X profile type	Complexity group	Sampling count
F1	87	E-W	177	12939.12	472.08	Irregular	Complex	148
F2	100	E-W	010	19040.98	704.13	Irregular	Complex	226
F3	72	E-W	162	4274.81	457.33	Asymmetric	Complex	51
F5	78	E-W	168	6874.81	647.01	Irregular	Complex	78
F12	100	E-W	010	2710.83	132.25	Double-peaked	Complex	33
F13	129	NW-SE	039	420.04	94.66	Symmetrical	Simple	7
F14	160	NW-SE	250	2371.18	632.63	Asymmetric	Complex	33
F16	42	NE-SW	132	6850.49	487.13	Irregular	Complex	82
F17	95	E-W	005	4191.74	323.09	Irregular	Complex	48
F20	135	NW-SE	225	3892.26	663.89	Asymmetric	Complex	48
F21	66	NE-SW	156	2030.03	496.55	Flat-topped	Simple	25
F23	133	NW-SE	223	1476.97	485.12	Symmetrical	Simple	22
F34	142	NW-SE	232	5078.15	446.97	Flat-topped	Simple	62
F41	62	NE-SW	152	6702.06	628.86	Irregular	Complex	77
F42	114	E-W	024	3432.02	260.57	Double-peaked	Complex	40
F49	60	NE-SW	150	1558.22	387.67	Symmetrical	Simple	19
F55	136	NW-SE	226	1765.19	328.58	Symmetrical	Simple	25
F63	144	NW-SE	234	2350.85	481.13	Flat-topped	Simple	31

Fault strikes and calculated dip azimuths are expressed in degrees (°), maximum fault lengths in metres (m), and maximum throws in feet (ft). Dip azimuths were derived from fault strike and interpreted dip polarity. Along-strike throw-distance (T-X) profiles were classified as symmetrical, asymmetric, double-peaked, flat-topped or irregular. Symmetrical and flat-topped profiles were grouped as simple, whereas asymmetric, double-peaked and irregular profiles were classified as complex. Sampling count represents the number of along-strike throw measurement positions per fault at the interpreted horizon represented by the corresponding profile.

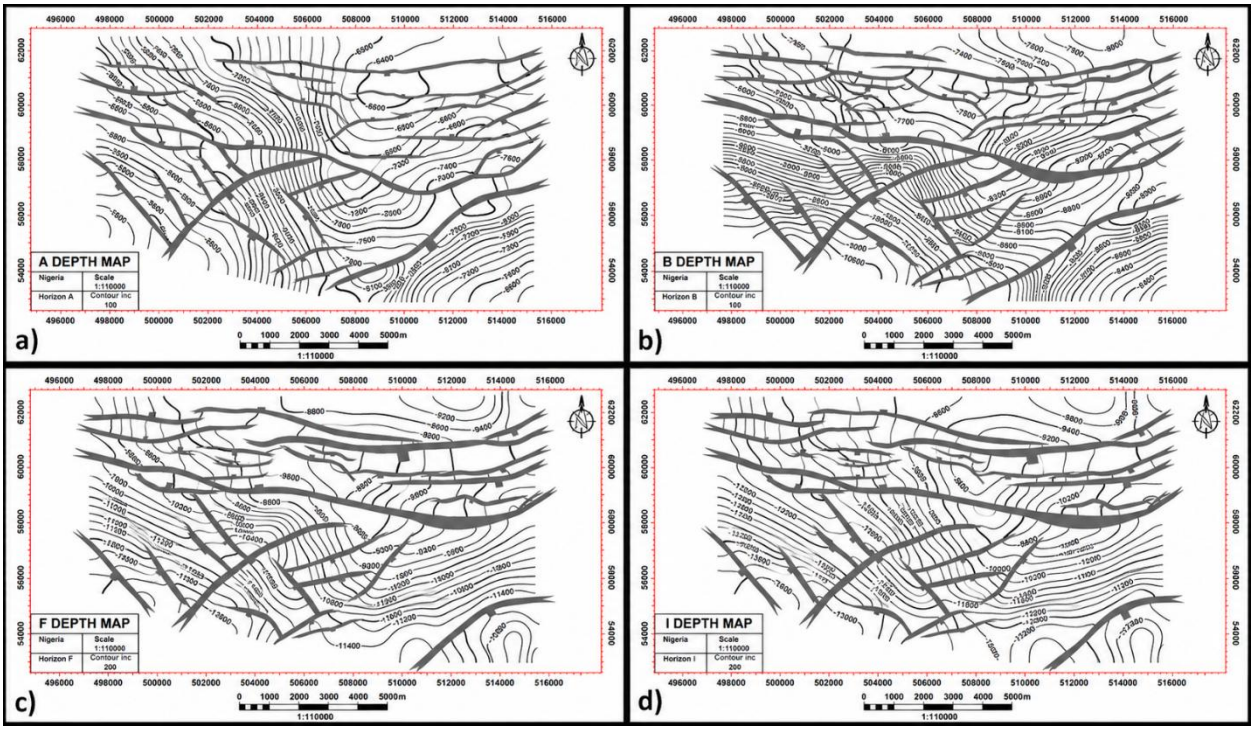


Fig. 3: Depth-structure maps of the TOYO Field showing the interpreted fault network at successive stratigraphic levels: (a) Horizon A, (b) Horizon B, (c) Horizon F and (d) Horizon I. Contours represent structural depth and illustrate changes in fault geometry and structural relief across the four mapped horizons

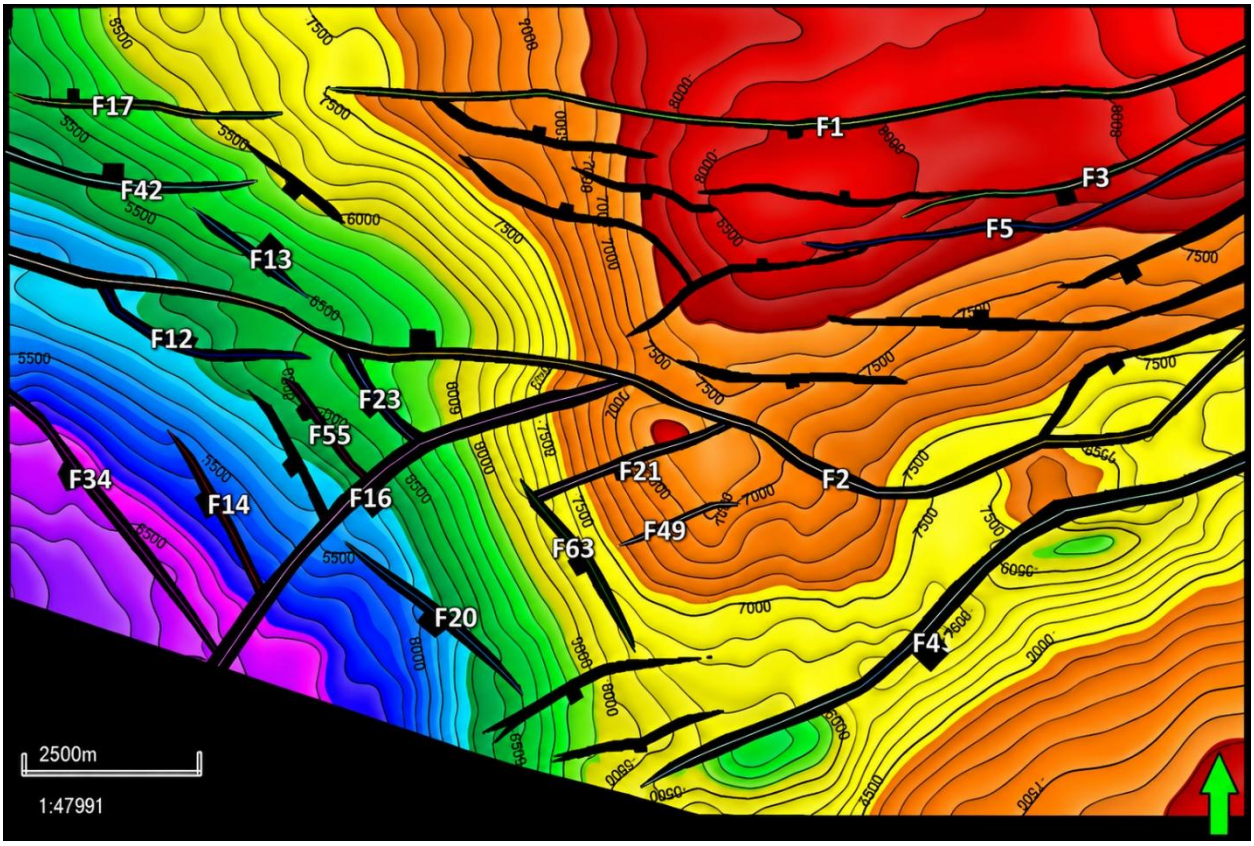


Fig. 4: Fault-polygon map of the TOYO Field showing the spatial distribution and map-view geometry of the principal faults selected for quantitative analysis, together with additional interpreted faults that define the broader structural framework. Background contours represent structural depth

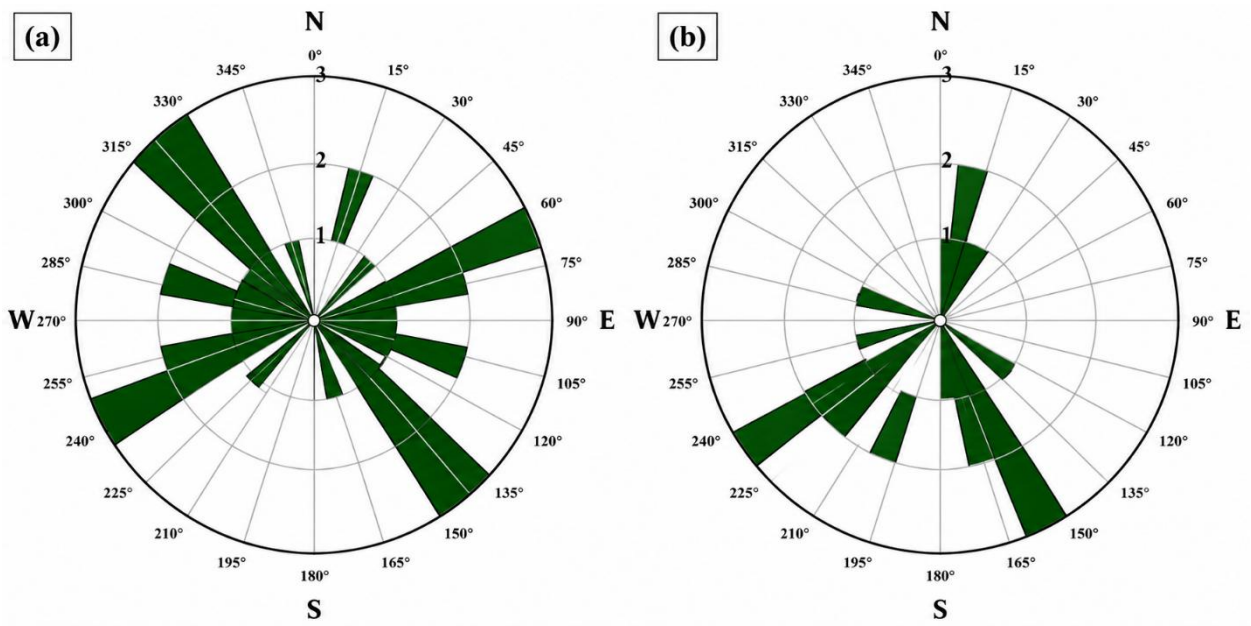


Fig. 5: Rose diagrams showing the orientation distribution of the 18 principal faults interpreted in the TOYO Field, Coastal Swamp Depobelt, Niger Delta. (a) Bidirectional fault-strike distribution represented as axial data, with equivalent orientations separated by 180°. (b) Unidirectional fault dip-azimuth distribution showing the interpreted northward- and southward-dipping fault populations. Rose diagrams were constructed using a 10° bin interval. Radial values represent frequency. The fault population is classified into three principal strike-orientation groups: E-W (n = 7), NE-SW (n = 4) and NW-SE (n = 7).

Fault-orientation analysis of the 18 interpreted faults identifies three broad orientation groups: E-W, NE-SW and NW-SE. The E-W and NW-SE groups each contain seven faults (38.9% of the analyzed population), whereas four faults (22.2%) are assigned to the NE-SW group. The rose diagram illustrates the axial nature of the strike data, such that orientations separated by 180° represent the same structural trend.

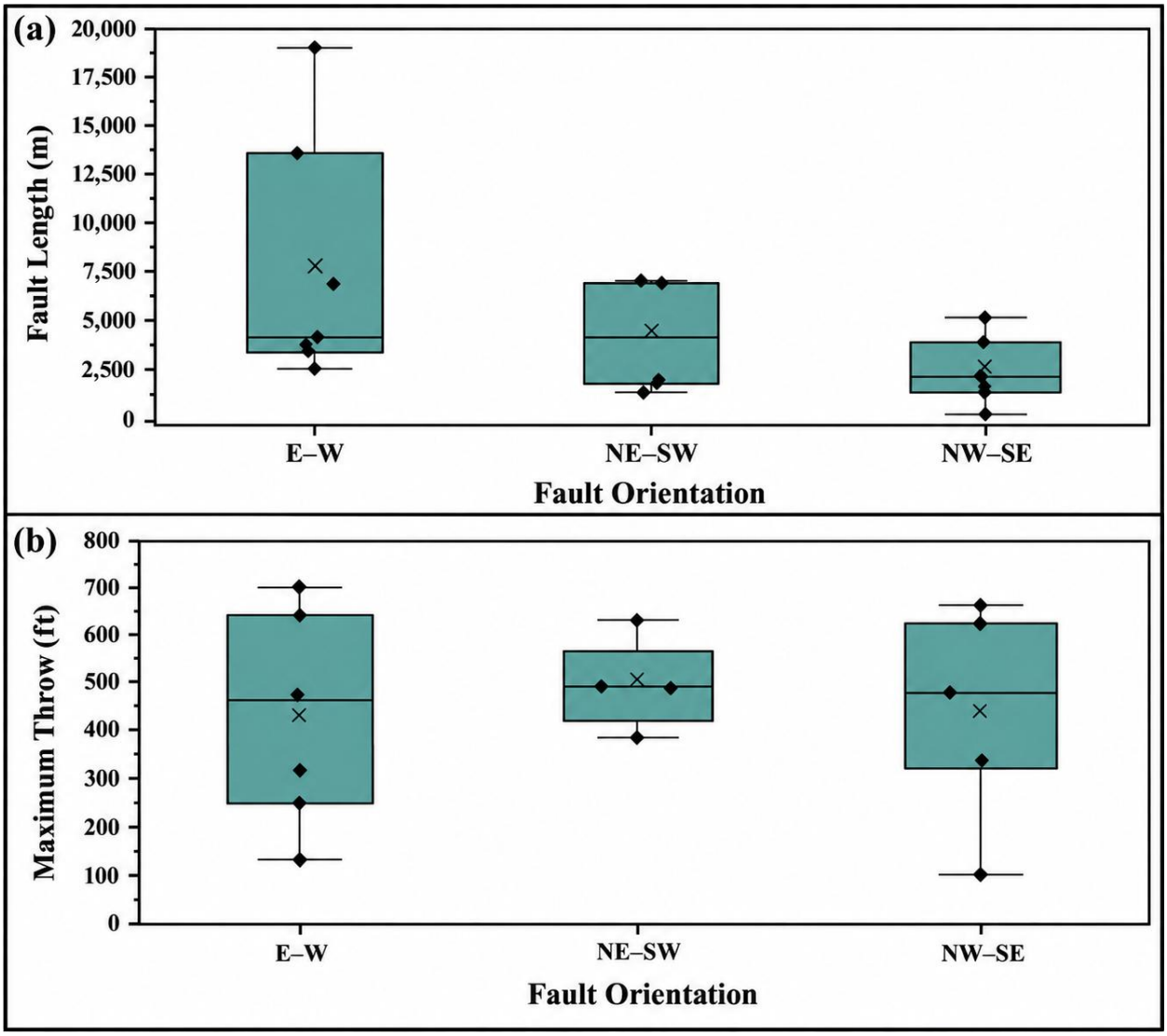


Fig. 6: Distribution of (a) fault length and (b) maximum throw among the E-W, NE-SW and NW-SE orientation groups. Boxes represent the interquartile range (IQR), horizontal lines within boxes indicate medians, whiskers extend to the most extreme values within 1.5 × IQR, and individual observations are shown as points. Kruskal-Wallis tests indicate no statistically significant differences among orientation groups for fault length ($H(2) = 5.786$, $p = 0.0554$) or maximum throw ($H(2) = 0.643$, $p = 0.7251$).

4.2 Along-strike displacement patterns (T-X)

Five T-X profile classes occur. Symmetrical profiles account for 22%, asymmetric profiles 17%, double-peaked profiles 11%, flat-topped profiles 17%, and irregular/complex profiles 33% of the 18-fault population.

When the T-X profiles were grouped into relatively simple (symmetrical and flat-topped; n = 7) and complex (asymmetric, double-peaked and irregular; n = 11) categories, maximum fault length differed significantly between the groups. The median maximum fault length was 1,765.19 m for the simple group and 4,274.81 m for the complex group (Mann-Whitney U = 6.0, exact two-sided p = 0.0019; rank-biserial effect magnitude = 0.844). In contrast, maximum throw did not differ significantly, with medians of 446.97 ft and 487.13 ft for the simple and complex groups, respectively (U = 25.0, exact two-sided p = 0.2463; rank-biserial effect magnitude = 0.351). These findings indicate an association between fault length and displacement-profile complexity in the analyzed population, but do not establish a causal relationship. Because longer faults generally have more measurement positions, sampling density may influence the identification and classification of profile irregularities; this effect remains to be tested through normalized-profile resampling.

Table 2: Mann-Whitney U test comparing fault size between simple and complex T-X displacement-profile groups

Variable	Simple profiles median	Complex profiles median	Mann-Whitney U	p-value	Rank-biserial effect size
Maximum fault length	1,765.19 m	4,274.81 m	6.0	0.0019	0.844
Maximum throw	446.97 ft	487.13 ft	25.0	0.2463	0.351

U denotes the Mann-Whitney statistic for the simple-profile group. P-values are exact and two-sided. Rank-biserial effect sizes are reported as absolute magnitudes; the signed correlation is negative when the simple group is the reference group because its values tend to be lower than those of the complex group. Statistical significance was assessed at $\alpha = 0.05$.

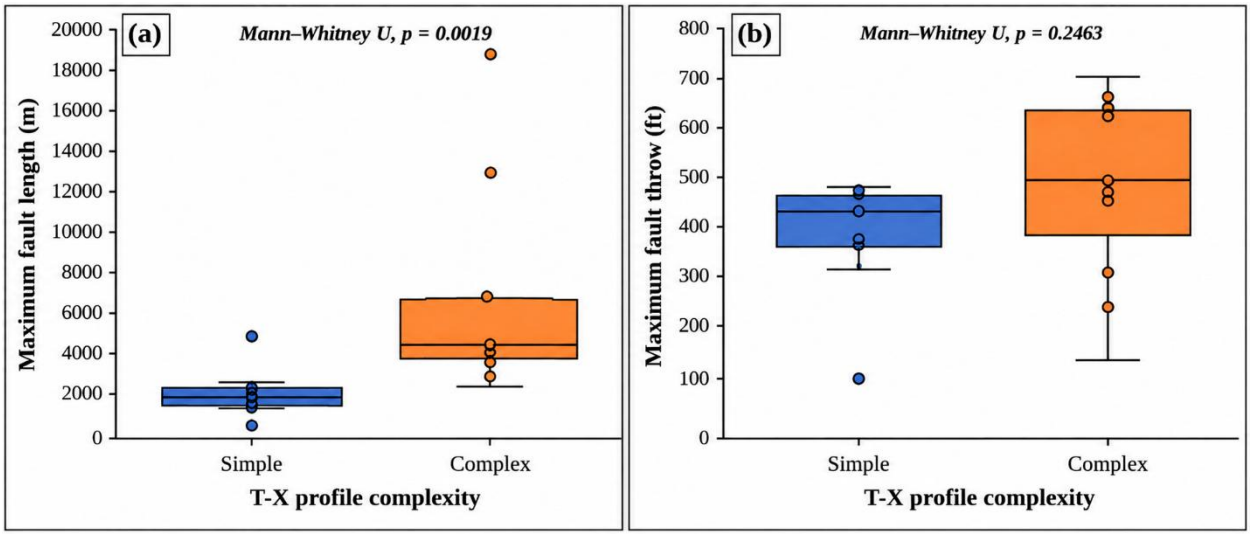


Fig. 7: Box-and-whisker plots comparing (a) maximum mapped fault length and (b) maximum fault throw between faults with simple and complex along-strike displacement (T-X) profiles in the TOYO Field. Simple profiles comprise symmetrical and flat-topped forms (n = 7), whereas complex profiles comprise asymmetric, double-peaked and irregular forms (n = 11). Boxes represent the interquartile range, horizontal lines within boxes indicate the median, whiskers extend to the most extreme values within 1.5 × IQR, and individual observations are shown as points. Group differences were evaluated using two-sided Mann-Whitney U tests.

A statistically significant association occurs between fault length and displacement-profile complexity. Several of the longest mapped faults, including F1, F2, F5, F16 and F41, exhibit irregular along-strike throw-distance (T-X) profiles characterized by substantial spatial variability in their measured throw distributions. F2, the longest structure at approximately 19 km, contains multiple throw maxima near 0.8, 3.2 and 6.5 km, together with another broad displacement high between approximately 13 and 18 km.

By contrast, F13, F23, F49 and F55 have approximately symmetrical bell-shaped profiles and are among the shorter structures. This association does not establish that the shorter faults are young or isolated. For example, F23 and F55, which define candidate relay R3, individually display relatively simple displacement profiles despite forming a geometrically overlapping fault pair.

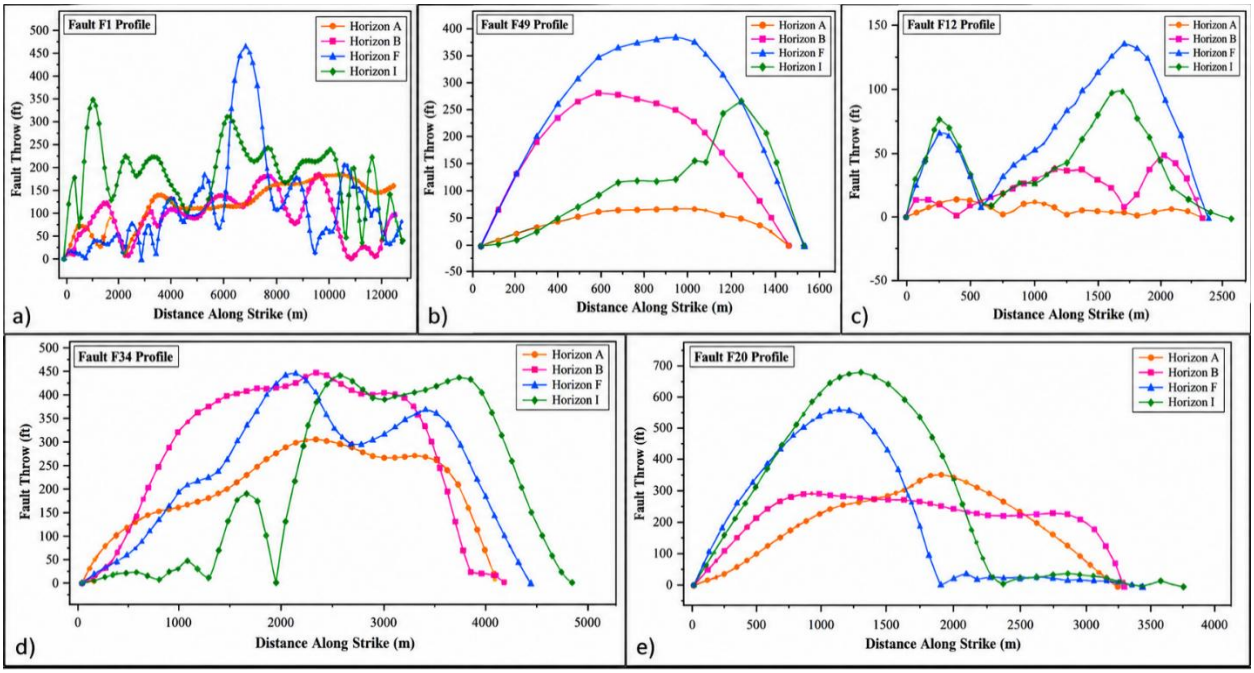


Fig. 8: Representative along-strike throw-distance (T-X) profiles illustrating contrasting throw-distribution geometries in the TOYO Field: (a) F1, irregular; (b) F49, symmetrical; (c) F12, double-peaked; (d) F34, flat-topped; and (e) F20, asymmetric.

4.3 Vertical displacement variation

Non-monotonic T-Z profiles dominate the dataset, occurring on 11 of 18 faults (61.1%). Expanding profiles characterize F3, F20 and F23; F34 and F42 are blocky; F13 is restricted to depth; and F41 displays an overall waning-with-depth pattern.

Several faults show local displacement maxima or minima around Horizon F. This recurring behaviour identifies Horizon F as an interval of enhanced displacement variability but does not establish its cause.

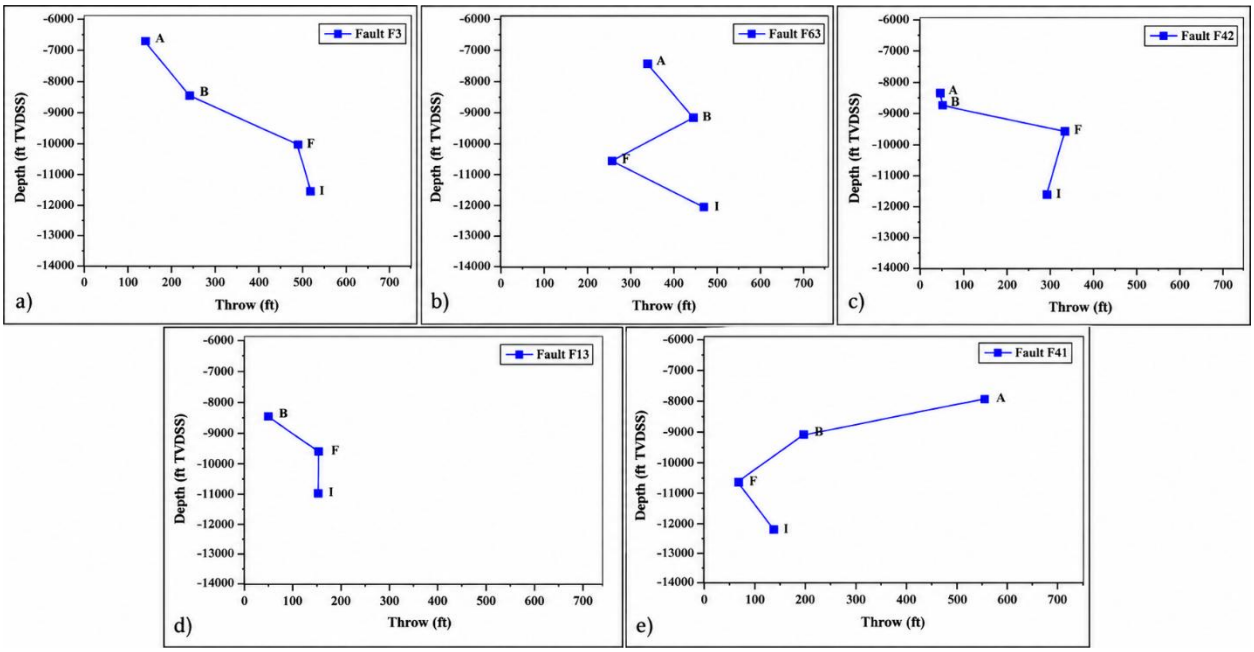


Fig. 9: Representative throw-depth (T-Z) profiles showing vertical displacement variability across Horizons A, B, F and I in selected TOYO Field faults. Depth is plotted on the vertical axis and throw on the horizontal axis. The profiles illustrate contrasting vertical displacement patterns, including non-monotonic, expanding, blocky, restricted-to-depth and waning-with-depth geometries

4.4 Displacement-length scaling

Displacement-length (D-L) scaling analysis of the 18 principal faults revealed positive relationships between fault length and maximum displacement across all four interpreted horizons (Fig. 10; Table 3). Because fault length (L) and maximum displacement (D_{max}) were already expressed in metres, both variables were used without further unit conversion. The $\log_{10}$ transformed datasets yielded regression slopes of 0.7084, 0.6322, 0.3366 and 0.7428 for Horizons A, B, F and I, respectively. The corresponding coefficients of determination (R^2) were 0.2666, 0.2318, 0.1800 and 0.3975.

Statistically significant positive relationships were obtained for Horizons A ($p = 0.0283$), B ($p = 0.0431$) and I ($p = 0.0050$), whereas the relationship for Horizon F was not statistically significant at the 0.05 level ($p = 0.0793$). Horizon I exhibited the highest coefficient of determination, while Horizon F showed the weakest relationship. The relatively low R^2 values indicate substantial scatter in the fault population, suggesting that fault length alone does not account for all observed variation in maximum displacement.

Table 3: Horizon-specific displacement-length regression statistics for the 18 principal faults in the TOYO Field.

Horizon	Scaling exponent (n)	R^2	P-value	Intercept (a)	Sample size (N)	95% CI for slope
A	0.708	0.267	0.0283	-0.4723	18	0.086 - 1.331
B	0.632	0.232	0.0431	-0.0618	18	0.022 - 1.242
F	0.337	0.180	0.0793	1.0604	18	-0.044 - 0.717
I	0.743	0.398	0.0050	-0.2743	18	0.258 - 1.227

The fitted scaling exponents were below unity for all four horizons. These relationships describe the observed fault population but do not independently establish a unique fault-growth mechanism or chronological sequence of fault development.

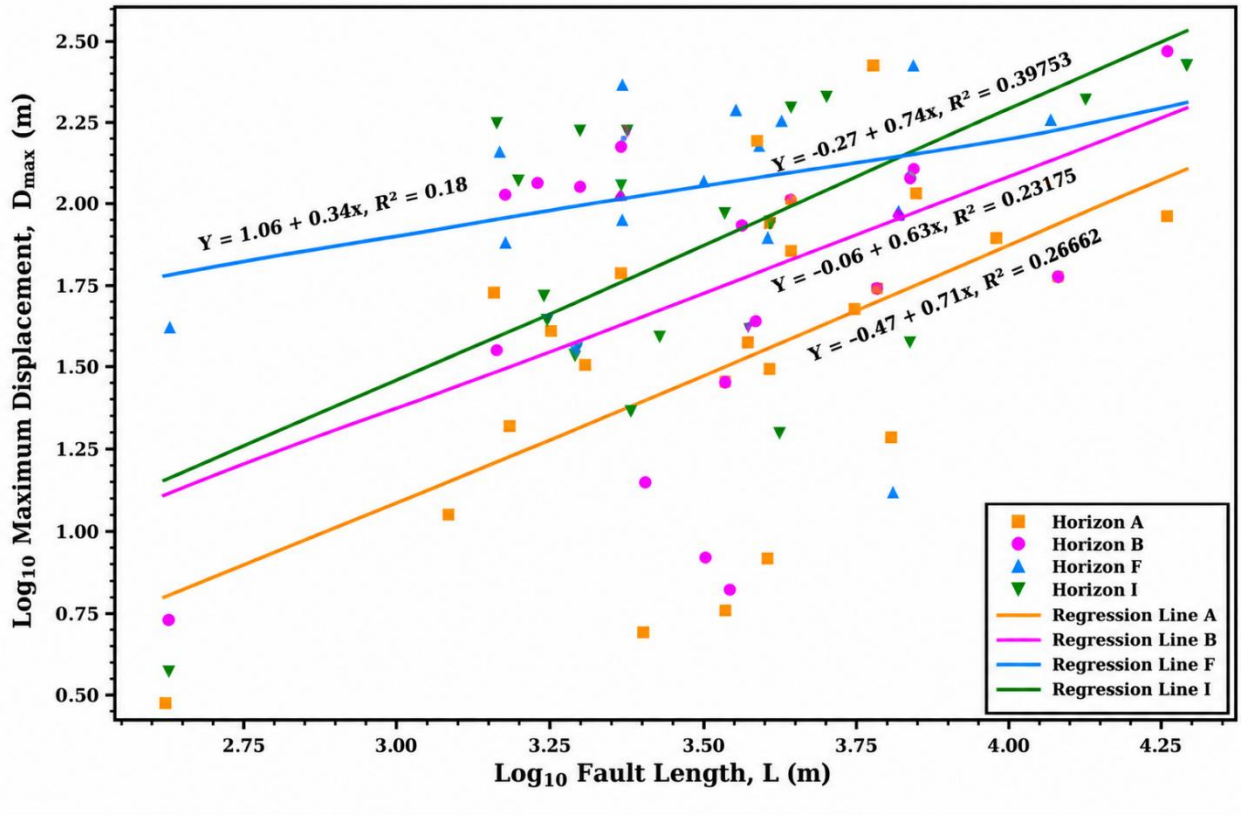


Fig. 10: Displacement-length (D-L) scaling relationships for 18 principal faults across Horizons A, B, F and I in the TOYO Field, Coastal Swamp Depobelt, Niger Delta. Fault length and maximum displacement are expressed in metres and plotted in log_{10} space. Solid lines represent horizon-specific least-squares linear regressions. The relationships are statistically significant for Horizons A, B and I ($p < 0.05$), but not for Horizon F ($p = 0.0793$)

4.5 Relay and interaction/linkage geometry

Four candidate relay relationships: R1 (F17-F42), R2 (F42-F13), R3 (F23-F55) and R4 (F3-F5) and four candidate interaction/linkage relationships: L1 (F1-F17), L2 (F2-F13), L3 (F2-F16) and L4 (F21-F49), were identified from the mapped fault network (Fig. 11). The candidate relays display positive geometrical overlap but differ substantially in the magnitude of overlap relative to separation. R1 has an overlap of 3476.30 m and separation of 1204.73 m (O/S = 2.89), R2 has an overlap of 914.88 m and separation of 341.83 m (O/S = 2.68), R3 has an overlap of 1652.26 m and separation of 665.53 m (O/S = 2.48), and R4 has an overlap of 4157.88 m and separation of 431.00 m (O/S = 9.65). R4 therefore exhibits the greatest geometrical overlap relative to separation, whereas R3 has the lowest O/S ratio.

Four additional relationships were classified as candidate interaction/linkage zones: L1 (F1-F17), L2 (F2-F13), L3 (F2-F16) and L4 (F21-F49) (Fig. 11). These relationships display map-view geometries characterized by convergence, close spatial association or apparent structural continuity between neighbouring fault segments, consistent with

stronger fault interaction or possible linkage. Where the corresponding faults are intersected by the available seismic section, individual fault surfaces remain distinguishable. Consequently, L1-L4 are treated as candidate interaction/linkage relationships rather than unequivocal evidence of hard linkage.

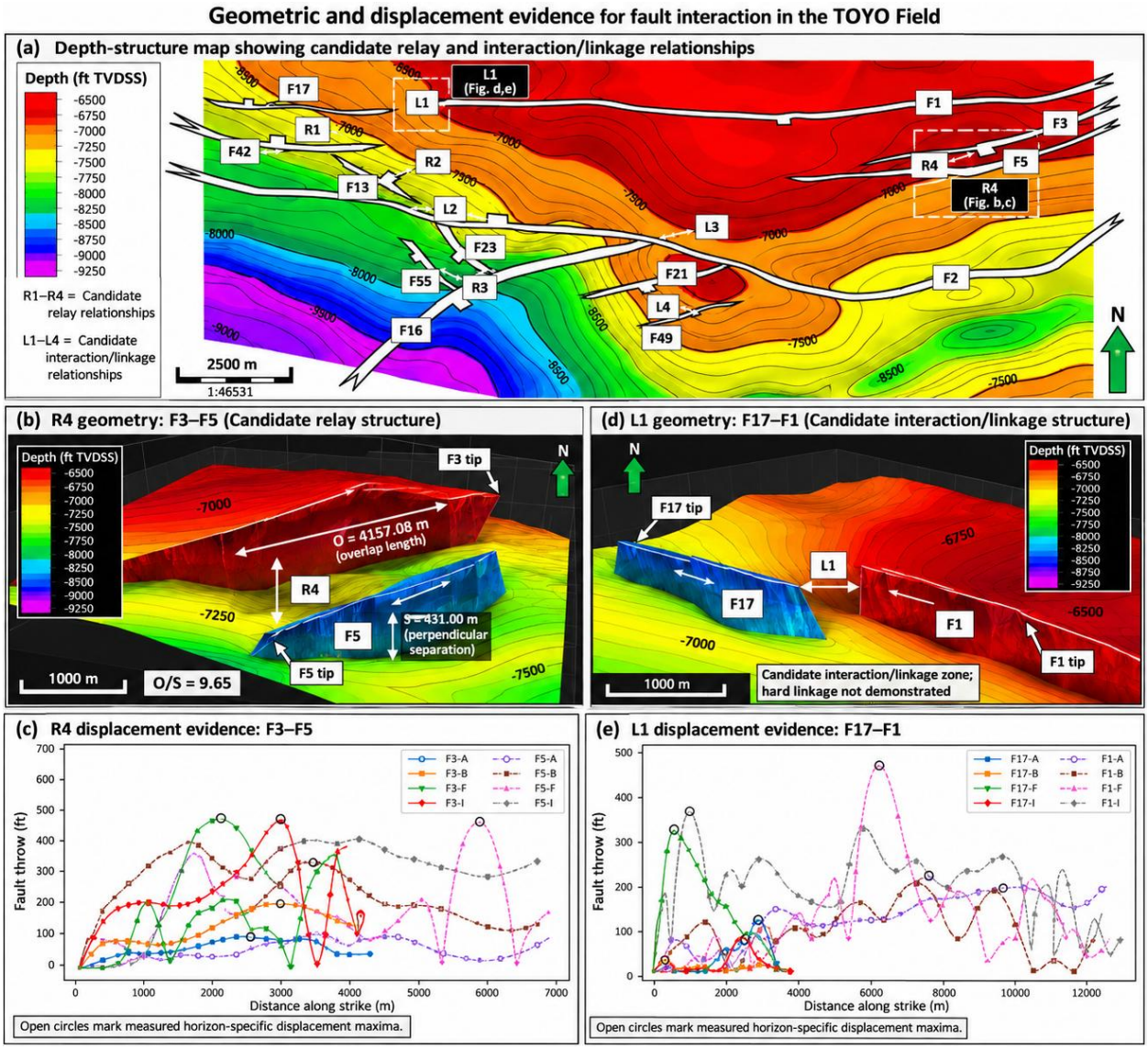


Fig. 11: Geometric and displacement evidence for fault interaction in the TOYO Field, Coastal Swamp Depobelt, Niger Delta. (a) Depth-structure map showing four candidate relay relationships (R1-R4) and four candidate interaction/linkage relationships (L1-L4). (b) Enlarged 3D view of relay R4 (F3-F5), showing fault overlap (O = 4157.88 m), separation (S = 431.00 m) and O/S ratio (9.65). (c) Corresponding along-strike throw-distance (T-X) profiles for F3 and F5 across Horizons A, B, F and I, with open circles indicating horizon-specific throw maxima. (d) Enlarged 3D view of candidate interaction/linkage L1 (F17-F1), illustrating fault proximity and possible interaction. (e) Corresponding T-X profiles showing along-strike throw variability in F17 and F1. Together, these observations suggest possible fault interaction and displacement transfer but do not independently establish physical linkage, transfer direction or a unique fault-growth history.

5. Discussion

5.1 From isolated fault growth to interaction

An idealized isolated normal fault commonly develops an approximately elliptical displacement distribution, expressed in map view as a broadly symmetrical displacement-distance profile with displacement decreasing toward the tips (Walsh and Watterson 1989; Cowie and Scholz 1992; Bürgmann et al. 1994; Nicol et al. 1996; Kim and Sanderson 2005). Progressive interaction can modify this distribution as neighbouring fault segments enter one another's stress fields. Relay zones may transfer displacement between overlapping normal-fault segments, while linkage points may be associated with displacement minima and increased complexity in displacement-distance profiles (Peacock and Sanderson 1991, 1994; Childs et al. 1995; Willemse et al. 1996).

The short, symmetrical TOYO faults F13, F23, F49 and F55 most closely resemble the geometric end-member expected for relatively simple displacement accumulation. They should not, however, be classified automatically as isolated faults. F23-F55 forms a mapped overlapping pair, demonstrating that an apparently simple individual T-X profile can coexist with geometric interaction.

This indicates that fault-growth stage cannot be assigned from T-X shape alone.

At the other end of the spectrum, the longest TOYO structures contain substantially more complicated displacement patterns. F2, for example, contains several displacement culminations separated by minima. Similar complex displacement distributions have been associated with interaction and linkage of component fault segments in natural and modelled fault systems (Peacock and Sanderson 1991; Imber et al. 2004).

The TOYO data are therefore consistent with but do not uniquely prove the interpretation that some long, irregular faults represent composite structures that have experienced stronger segment interaction and displacement redistribution.

5.2 Segment interaction and displacement transfer

The statistical relationship between fault length and T-X profile complexity provides quantitative support for the observed association between fault size and along-strike displacement variability. Complex-profile faults are significantly longer than faults with simple profiles ($U = 6.0$, $p = 0.0019$), and the large rank-biserial effect size ($rrb = 0.844$) indicates that the difference is substantial rather than merely a consequence of the small sample size. In contrast, maximum throw does not differ significantly between the two groups ($p = 0.2463$). Thus, within the analyzed TOYO fault population, along-strike throw-profile complexity shows a statistically significant association with maximum mapped fault length, whereas the corresponding association with maximum throw is not statistically significant.

The association between fault length and profile complexity is compatible with the possibility that longer faults preserve more complex displacement distributions as a result of segment interaction and structural integration. The mapped relay and candidate interaction/linkage relationships provide additional geometric observations consistent

with this interpretation. However, because measurement density increases with fault length, the contribution of sampling effects remains unresolved. Neither fault length nor displacement-profile complexity alone establishes that a fault formed through segment linkage or that displacement was transferred between segments.

Fault interaction can begin before physical linkage. As propagating fault tips approach one another, their stress fields interact and may alter the spatial distribution of displacement (Crider and Pollard 1998; Gupta and Scholz 2000). Mechanical and numerical models demonstrate that stress interaction between overlapping normal faults can promote displacement perturbation, relay-zone deformation and eventual linkage without requiring the faults to be initially connected (Willemse et al. 1996; Crider and Pollard 1998; Gupta and Scholz 2000; Imber et al. 2004; Nicol et al. 2010).

Several TOYO observations are compatible with this stage. F3, F14 and F20 display asymmetric profiles, whereas F12 and F42 display double displacement maxima. F42 contains a displacement minimum at approximately 2.1 km along strike and participates in candidate relay R1 (F17-F42), while F3 participates in candidate relay R4 (F3-F5). The spatial coincidence between complex displacement patterns and mapped neighbouring structures is consistent with fault interaction, although neither profile geometry nor spatial association alone demonstrates physical linkage.

5.3 Soft linkage and relay-ramp development

Where neighbouring normal-fault segments overlap without forming an unequivocally continuous fault surface, displacement may be transferred through deformation of the intervening relay zone (Peacock and Sanderson 1991, 1994; Childs et al. 1995; Peacock 2002; Walsh et al. 2003). Relay structures therefore represent important sites of kinematic interaction between adjacent fault segments.

Four candidate relay relationships were identified in the TOYO Field: R1 (F17-F42), R2 (F42-F13), R3 (F23-F55) and R4 (F3-F5). All four display positive geometrical overlap, but the magnitude of overlap relative to separation varies substantially. R1 has an O/S ratio of 2.89, R2 = 2.68, R3 = 2.48 and R4 = 9.65. R4 therefore displays the greatest geometrical overlap relative to separation, whereas R3 has the lowest ratio.

The association of these mapped overlap geometries with spatial variations in displacement is consistent with fault interaction and displacement transfer. However, the O/S ratios are used here as descriptive measures of relay geometry rather than as thresholds for relay maturity or hard linkage. The mapped relationships are therefore interpreted as candidate relay structures rather than as evidence of a fixed evolutionary stage.

5.4 Candidate interaction/linkage and possible relay breaching

Progressive deformation of relay zones can ultimately produce breaching structures and, in some cases, hard linkage between previously separate fault segments (Peacock and Sanderson 1994; Peacock 2002; Walsh et al. 2003; Imber et al. 2004).

The candidate interaction/linkage relationships L1 (F1-F17), L2 (F2-F13), L3 (F2-F16) and L4 (F21-F49) represent locations where the mapped fault geometry is compatible with stronger segment interaction or possible linkage.

However, map-view convergence or apparent continuity alone does not demonstrate physical connection between fault surfaces. Where the relevant faults are intersected by the available seismic section, individual fault surfaces remain distinguishable; therefore, these relationships are interpreted cautiously as candidate interaction/linkage zones rather than confirmed hard-linked structures. Apparent map-view continuity may represent close interaction, overlap, incipient linkage or a connecting structure that is not unequivocally resolved by the available seismic data.

Accordingly, the TOYO fault network is interpreted as preserving a spectrum of interaction states ranging from geometrically overlapping relay relationships (R1-R4) to candidate interaction/linkage relationships (L1-L4), rather than a simple division between isolated and fully linked faults.

5.5 D-L variability and possible displacement redistribution

A conventional fault-growth model predicts broadly coupled increases in displacement and fault dimensions (Cowie and Scholz 1992; Dawers et al. 1993; Scholz et al. 1993). Alternative growth models, however, indicate that fault length may become established comparatively early, followed by a longer period dominated by displacement accumulation with relatively limited additional tip propagation (Walsh et al. 2002; Nicol et al. 2005; Rotevatn et al. 2019). Such behaviour provides one possible explanation for why natural fault populations may display substantial scatter in D-L space.

All four horizons show positive D-L relationships, but the relatively low R^2 values (0.180-0.398) indicate that fault length alone explains only a limited proportion of the variability in maximum displacement. This scatter does not, by itself, demonstrate displacement redistribution. Instead, several processes may contribute, including segmentation and linkage, mechanical stratigraphy, fault reactivation and measurement or seismic-resolution effects (Cartwright et al. 1995; Kim and Sanderson 2005; Torabi and Berg 2011; Soliva et al. 2005). Importantly, the TOYO population independently contains mapped relay and candidate interaction/linkage relationships together with asymmetric, multi-peaked and irregular T-X profiles. The coexistence of these observations makes displacement redistribution associated with fault interaction and possible linkage a plausible contributor to the observed D-L variability, although it cannot be uniquely demonstrated from the scaling relationships alone. The TOYO population is therefore inconsistent with a simple model in which every fault evolved along an identical isolated D-L trajectory.

These departures should therefore not be assigned uniquely to a single process or interpreted automatically as indicators of fault maturity.

5.6 A fault-growth spectrum for the TOYO Field

The integrated observations permit a conceptual, rather than chronological, growth spectrum:

Stage 1: Relatively simple fault segments: Faults with comparatively simple displacement distributions represent the closest TOYO analogues to relatively uncomplicated segment geometries.

Stage 2: Segment propagation: Continued lateral and vertical propagation increases fault dimensions and displacement while neighbouring segments remain structurally distinguishable.

Stage 3: Interaction and relay development: Approaching or overlapping segments enter one another's stress fields, producing displacement perturbations and relay-zone development through which displacement may be transferred.

Stage 4: Relay breaching and possible linkage: Continued deformation may promote breaching of relay zones and increased structural integration. The TOYO L1-L4 relationships are treated as candidate interaction/linkage zones rather than confirmed examples of hard linkage.

Stage 5: Structural integration and displacement redistribution: More integrated fault systems may retain complex or multi-peaked displacement distributions inherited from earlier segmentation and interaction while displacement continues to accumulate along the composite structure.

This five-stage framework represents a conceptual fault-growth spectrum derived from the integrated TOYO observations and established models of fault propagation, interaction, relay development and linkage (Peacock and Sanderson 1991, 1994; Childs et al. 1995; Crider and Pollard 1998; Peacock 2002; Walsh et al. 2003; Imber et al. 2004; Childs et al. 2017; Rotevatn et al. 2019). It should not be interpreted as a uniquely reconstructed chronological sequence followed by every individual fault in the field.

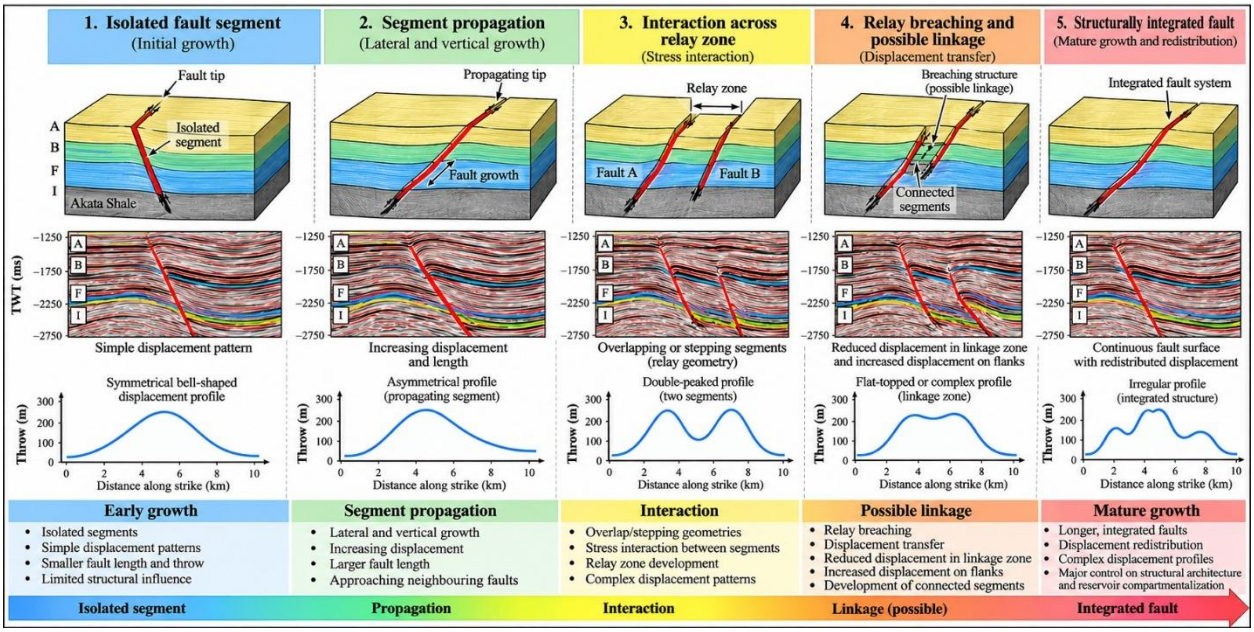


Fig. 12: Conceptual fault-growth spectrum for the TOYO Field integrating mapped fault geometry, displacement distributions and relay/interaction relationships. The model progresses from (1) relatively simple fault segments, through (2) lateral and vertical segment propagation, (3) segment interaction, relay development and displacement transfer, (4) relay breaching and possible linkage, to (5) structural integration and displacement redistribution. The model represents a conceptual spectrum of fault-growth relationships rather than a uniquely reconstructed chronological sequence for individual TOYO faults. Hard linkage is presented as a possible evolutionary state and is not inferred for all mapped candidate interaction/linkage relationships (L1-L4).

5.7 Significance of Horizon F

Horizon F is structurally distinctive within the analyzed dataset, showing the lowest D-L exponent (0.337), the lowest coefficient of determination ($R^2 = 0.180$) and several local displacement anomalies in the T-Z profiles. Mechanical stratigraphy can influence fault propagation and displacement distribution where fault tips encounter contrasting mechanical layers (Wilkins and Gross 2002; Soliva and Benedicto 2005; Soliva et al. 2005). However, the present study did not systematically correlate the observed Horizon F anomalies with sand-shale boundaries or quantify mechanical-property contrasts. A mechanical-stratigraphic influence therefore remains a plausible hypothesis rather than a demonstrated control.

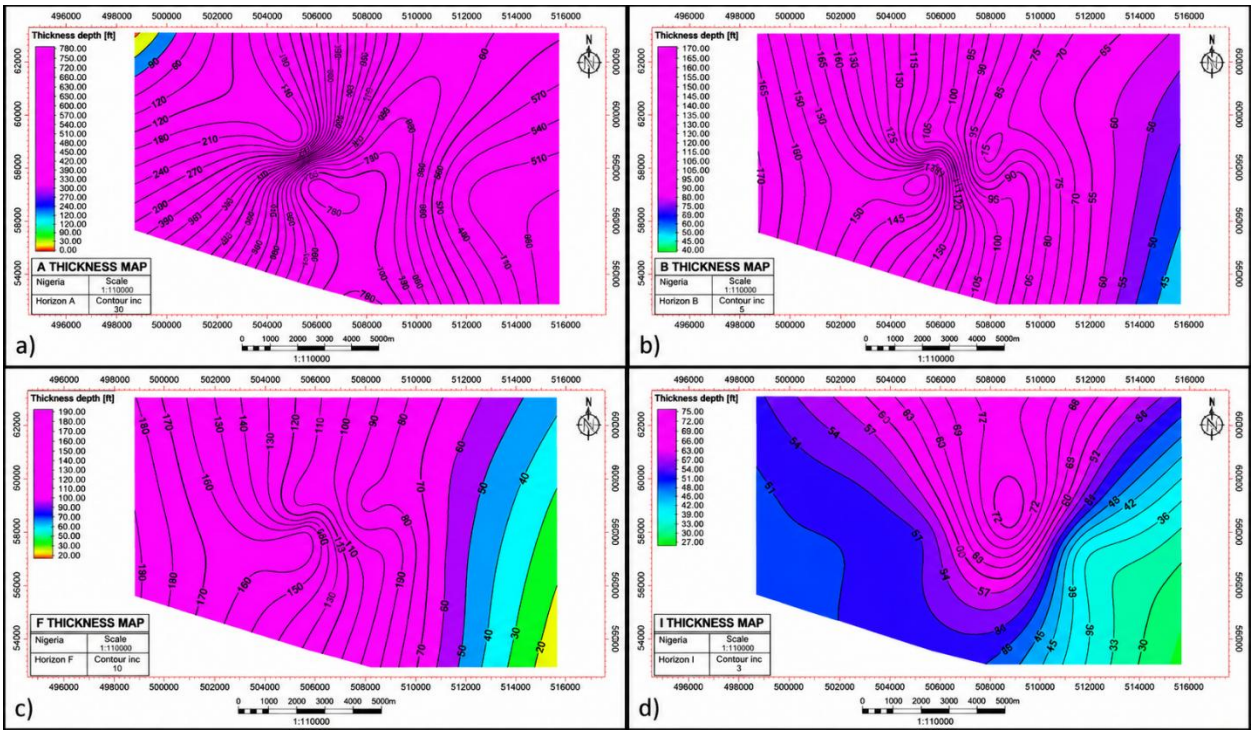


Fig. 13: Isochore maps of the TOYO Field showing spatial variations in interval thickness associated with Horizons (a) A, (b) B, (c) F and (d) I. Contour intervals are 30 ft, 5 ft, 10 ft and 3 ft for Horizons A, B, F and I, respectively. Thickness variations are compared with the mapped structural framework to evaluate possible spatial relationships between faulting and differential stratigraphic accommodation.

5.8 Implications for Niger Delta growth-fault evolution

The TOYO fault network fits a broader pattern documented in deltaic normal-fault systems in which final fault architecture can preserve evidence of earlier segmentation even after fault systems become geometrically integrated. Studies of active extensional basins similarly emphasize that fault propagation, linkage and interaction can exert major controls on basin architecture and syn-tectonic accommodation (Gawthorpe and Leeder 2000). In the western Niger Delta, Fazli Khani and Back (2012) documented temporal and lateral variations in growth-fault activity, while Fazlikhani and Back (2015) used 3D seismic data to document lateral propagation and linkage of initially separate

fault segments into an approximately 15-km-long master fault. Fazlikhani et al. (2017) further showed that linkage of gravity-driven listric normal faults is dynamically coupled to hanging-wall rollover development.

Similarly, Umar et al. (2019) documented isolated and coherently linked normal faults, relay ramps and complex throw distributions in an onshore Niger Delta field, demonstrating the importance of segment interaction and displacement transfer in regional growth-fault systems. The TOYO Field extends these observations by showing that relatively simple displacement profiles coexist within the same fault population with irregular and multi-peaked structures, geometrically overlapping relay candidates and candidate interaction/linkage relationships.

The integrated structural and displacement evidence suggests that spatially variable segment interaction and structural integration provide a more informative explanation of the observed TOYO fault-network heterogeneity than fault orientation considered independently. Although fault length and maximum throw do not differ significantly among the three orientation groups at the 0.05 level, these statistical results do not exclude orientation-dependent influences on fault development. Rather, the combination of displacement-profile variability, mapped relay geometries, candidate interaction/linkage relationships and displacement-length scaling indicates that fault-network architecture reflects several interacting structural controls. The available evidence therefore supports a conceptual framework of spatially variable fault interaction without uniquely establishing the evolutionary sequence or linkage history of individual structures.

5.9 Implications for reservoir compartmentalization

Fault-interaction state has direct implications for the geometry of potential reservoir compartments. An isolated fault segment may produce a comparatively simple reservoir offset, whereas interacting but soft-linked segments can generate relay zones in which stratigraphic continuity and potential communication pathways differ from those associated with a continuous through-going fault. Progressive relay breaching may increase structural segmentation, while development of a hard-linked composite fault could produce a more laterally continuous structural compartment boundary. In addition, displacement redistribution along interacting or composite faults may generate spatial variations in reservoir juxtaposition and potential seal behaviour along the same structure. These geometric predictions should be separated from hydraulic fault-seal behaviour, which also depends on fault-zone architecture, juxtaposition and fault-rock properties (Caine et al. 1996; Yielding et al. 1997).

Within the TOYO Field, these relationships generate a structurally complex northeastern domain around F1-F3-F5, a central-southern domain containing additional interacting structures, a southwestern domain dominated by shorter faults, and a northwestern antithetic cluster involving F12, F13, F17 and F42. The mapped relay and candidate interaction/linkage relationships therefore provide a structural framework for predicting where reservoir continuity and compartment geometry may change across the field.

These interpretations are structural predictions rather than demonstrated flow behaviour. Fault juxtaposition analysis, shale-gouge ratio or other fault-seal metrics, pressure data and production histories would be required to determine whether individual faults and relay zones act as transmissive pathways or sealing compartment boundaries.

Nevertheless, identifying the interaction state provides a useful basis for prioritizing such analyses during reservoir characterization and development planning.

5.10 Limitations

Four principal limitations constrain the interpretation of the present study.

First, only 18 of 64 interpreted faults were quantitatively analyzed, biasing the dataset toward structures with sufficient seismic continuity.

Second, the four stratigraphic horizons provide too few temporal markers to reconstruct detailed propagation chronology.

Third, seismic resolution introduces uncertainty in fault-tip position, small throws and apparent segmentation.

Fourth, present-day geometry cannot uniquely distinguish between soft linkage, hard linkage and inherited segmentation without direct seismic evidence of connecting fault traces.

An additional limitation concerns the potential influence of measurement density on the classification of along-strike displacement profiles. Longer faults may contain more measurement positions and consequently provide greater opportunities for identifying multiple displacement maxima and local irregularities. This sampling effect could contribute to the observed statistical association between fault length and profile complexity. Future investigations should evaluate the robustness of this relationship using displacement profiles resampled at comparable normalized along-strike positions and, where possible, sensitivity tests involving alternative complexity classifications. Higher-resolution seismic interpretation, additional stratigraphic markers and independent fault-seal or dynamic reservoir data would further constrain the interpretation of fault interaction, linkage and reservoir connectivity.

6 Conclusions

1. The TOYO Field contains a heterogeneous normal-fault network comprising E-W, NE-SW and NW-SE structures with mapped lengths ranging from approximately 0.42 to 19.0 km. Although descriptive differences occur among the orientation groups, Kruskal-Wallis tests did not identify statistically significant differences in fault length ($H(2) = 5.786$, $p = 0.0554$) or maximum throw ($H(2) = 0.643$, $p = 0.7251$) at the 0.05 significance level. These results suggest that fault orientation considered independently is insufficient to account for the observed fault-network heterogeneity, although orientation-dependent geological influences cannot be excluded.

2. Along-strike throw profiles range from relatively simple symmetrical and flat-topped forms to asymmetric, double-peaked and irregular geometries. Complex-profile faults have greater median mapped lengths than simple-profile faults (4.27 versus 1.77 km; $U = 6.0$, $p = 0.0019$; rank-biserial correlation = 0.844), whereas maximum throw does not differ significantly between the groups ($p = 0.2463$). These results identify a statistical association between fault length and profile complexity in the analyzed population. However, the strong relationship between fault length and measurement count means that the influence of sampling density remains unresolved. The observed fault geometries are consistent with spatially variable interaction, but do not establish a unique fault-growth sequence or prove displacement transfer.
3. Non-monotonic T-Z profiles dominate the population (11/18; 61.1%), indicating substantial vertical variability in displacement accumulation. Recurrent displacement anomalies around Horizon F identify it as a structurally distinctive interval, although a mechanical-stratigraphic origin remains untested.

4. Positive D-L relationships occur at all four horizons, but scaling exponents of 0.34-0.74 and R^2 values of 0.180-0.398 indicate considerable population scatter. Fault length alone therefore explains only a limited proportion of the variability in maximum displacement, and the TOYO fault population cannot be described adequately by a single simple displacement-length growth trajectory.

5. Four candidate relay relationships (R1-R4) and four candidate interaction/linkage relationships (L1-L4) were identified. The relay candidates have O/S ratios of 2.48-9.65, with R4 (F3-F5) showing the greatest overlap relative to separation. The L1-L4 relationships display map-view geometries consistent with stronger fault interaction or possible linkage, but the available seismic evidence does not unequivocally demonstrate hard linkage.

6. Collectively, the observations are compatible with a conceptual spectrum from relatively simple fault segments through propagation, interaction and relay development to relay breaching, possible structural linkage and displacement redistribution. This represents a conceptual growth framework rather than a uniquely reconstructed chronology for individual TOYO faults.

7. Spatially variable degrees of fault interaction and structural integration are associated with a heterogeneous structural compartment framework across the TOYO Field. The mapped architecture therefore provides a

basis for reservoir compartment assessment, but hydraulic connectivity and fault-seal behaviour require quantitative juxtaposition and fault-seal analysis together with pressure and/or production data.

References

Bürgmann R, Pollard DD, Martel SJ (1994) Slip distributions on faults: Effects of stress gradients, inelastic deformation, heterogeneous host-rock stiffness, and fault interaction. Journal of Structural Geology 16:1675-1690. https://doi.org/10.1016/0191-8141(94)90134-1

Caine JS, Evans JP, Forster CB (1996) Fault zone architecture and permeability structure. Geology 24:1025-1028. https://doi.org/10.1130/0091-7613(1996)024<1025:FZAAPS>2.3.CO;2

Cartwright JA, Trudgill BD, Mansfield CS (1995) Fault growth by segment linkage: An explanation for scatter in maximum displacement and trace length data from the Canyonlands Grabens of SE Utah. Journal of Structural Geology 17:1319-1326. https://doi.org/10.1016/0191-8141(95)00033-A

Childs C, Holdsworth RE, Jackson CAL, Manzocchi T, Walsh JJ, Yielding G (2017) Introduction to the geometry and growth of normal faults. Geological Society, London, Special Publications 439:1-9. https://doi.org/10.1144/SP439.24

Childs C, Watterson J, Walsh JJ (1995) Fault overlap zones within developing normal fault systems. Journal of the Geological Society 152:535-549. https://doi.org/10.1144/gsjgs.152.3.0535

Corredor F, Shaw JH, Bilotti F (2005) Structural styles in the deep-water fold and thrust belts of the Niger Delta. AAPG Bulletin 89:753-780. https://doi.org/10.1306/02170504074

Cowie PA, Scholz CH (1992) Displacement-length scaling relationship for faults: Data synthesis and discussion. Journal of Structural Geology 14:1149-1156. https://doi.org/10.1016/0191-8141(92)90066-6

Crider JG, Pollard DD (1998) Fault linkage: Three-dimensional mechanical interaction between echelon normal faults. Journal of Geophysical Research: Solid Earth 103:24373-24391. https://doi.org/10.1029/98JB01353

Dawers NH, Anders MH, Scholz CH (1993) Growth of normal faults: Displacement-length scaling. Geology 21:1107-1110. https://doi.org/10.1130/0091-7613(1993)021<1107:GONFDL>2.3.CO;2

Doust H, Omatsola E (1990) Niger Delta. In: Edwards JD, Santogrossi PA (eds) Divergent/passive margin basins. AAPG Memoir 48. American Association of Petroleum Geologists, Tulsa, pp 201-238.

Evamy BD, Haremboure J, Kamerling P, Knaap WA, Molloy FA, Rowlands PH (1978) Hydrocarbon habitat of Tertiary Niger Delta. AAPG Bulletin 62:1-39

Fazli Khani H, Back S (2012) Temporal and lateral variation in the development of growth faults and growth strata in western Niger Delta, Nigeria. AAPG Bulletin 96:595-614. https://doi.org/10.1306/08291111023

Fazlikhani H, Back S (2015) The influence of pre-existing structure on the growth of syn-sedimentary normal faults in a deltaic setting, Niger Delta. Journal of Structural Geology 73:18-32. https://doi.org/10.1016/j.jsg.2015.01.011

Fazlikhani H, Back S, Kukla PA, Fossen H (2017) Interaction between gravity-driven listric normal fault linkage and their hanging-wall rollover development: A case study from the western Niger Delta, Nigeria. Geological Society, London, Special Publications 439:169-186. https://doi.org/10.1144/SP439.20

Gawthorpe RL, Leeder MR (2000) Tectono-sedimentary evolution of active extensional basins. Basin Research 12:195-218. https://doi.org/10.1111/j.1365-2117.2000.00121.x

Gupta A, Scholz CH (2000) A model of normal fault interaction based on observations and theory. Journal of Structural Geology 22:865-879. https://doi.org/10.1016/S0191-8141(00)00011-0

Imber J, Tuckwell GW, Childs C, Walsh JJ, Manzocchi T, Heath AE, Bonson CG, Strand J (2004) Three-dimensional distinct element modelling of relay growth and breaching along normal faults. Journal of Structural Geology 26:1897-1911. https://doi.org/10.1016/j.jsg.2004.02.010

Kim YS, Sanderson DJ (2005) The relationship between displacement and length of faults: A review. Earth-Science Reviews 68:317-334. https://doi.org/10.1016/j.earscirev.2004.06.003

Nicol A, Walsh JJ, Berryman K, Nodder S (2005) Growth of a normal fault by the accumulation of slip over millions of years. Journal of Structural Geology 27:327-342. https://doi.org/10.1016/j.jsg.2004.09.002

Nicol A, Walsh JJ, Villamor P, Seebeck H, Berryman KR (2010) Normal fault interactions, paleoearthquakes and growth in an active rift. Journal of Structural Geology 32:1101-1113. https://doi.org/10.1016/j.jsg.2010.06.018

Nicol A, Watterson J, Walsh JJ, Childs C (1996) The shapes, major axis orientations and displacement patterns of fault surfaces. Journal of Structural Geology 18:235-248. https://doi.org/10.1016/S0191-8141(96)80047-2

Peacock D C P (2002) Propagation, interaction and linkage in normal fault systems. Earth-Science Reviews 58:121-142. https://doi.org/10.1016/S0012-8252(01)00085-X

Peacock DCP, Sanderson DJ (1991) Displacements, segment linkage and relay ramps in normal fault zones. Journal of Structural Geology 13:721-733. https://doi.org/10.1016/0191-8141(91)90033-F

Peacock DCP, Sanderson DJ (1994) Geometry and development of relay ramps in normal fault systems. AAPG Bulletin 78:147-165. https://doi.org/10.1306/BDFF9046-1718-11D7-8645000102C1865D

Rotevatn A, Jackson CAL, Tvedt ABM, Bell RE, Blækkan I (2019) How do normal faults grow? Journal of Structural Geology 125:174-184. https://doi.org/10.1016/j.jsg.2018.08.005

Scholz CH, Dawers NH, Yu JZ, Anders MH, Cowie PA (1993) Fault growth and fault scaling laws: Preliminary results. Journal of Geophysical Research: Solid Earth 98:21951-21961. https://doi.org/10.1029/93JB01008

Soliva R, Benedicto A (2005) Geometry, scaling relations and spacing of vertically restricted normal faults. Journal of Structural Geology 27:317-325. https://doi.org/10.1016/j.jsg.2004.08.010

Soliva R, Schultz RA, Benedicto A (2005) Three-dimensional displacement-length scaling and maximum dimension of normal faults in layered rocks. Geophysical Research Letters 32:L16302. https://doi.org/10.1029/2005GL023007

Torabi A, Berg SS (2011) Scaling of fault attributes: A review. Marine and Petroleum Geology 28:1444-1460. https://doi.org/10.1016/j.marpetgeo.2011.04.003

Tuttle MLW, Charpentier RR, Brownfield ME (1999) The Niger Delta petroleum system: Niger Delta Province, Nigeria, Cameroon, and Equatorial Guinea, Africa. U.S. Geological Survey Open-File Report 99-50-H. https://doi.org/10.3133/ofr9950H

Umar BA, Gholami R, Nayak P, Downey WS, Shah AA (2019) Normal fault geometrical trends and interactions in an onshore oilfield Niger Delta Basin, Nigeria. Journal of Petroleum Science and Engineering 177:579-593. https://doi.org/10.1016/j.petrol.2019.01.056

Walsh JJ, Bailey WR, Childs C, Nicol A, Bonson CG (2003) Formation of segmented normal faults: A 3-D perspective. Journal of Structural Geology 25:1251-1262. https://doi.org/10.1016/S0191-8141(02)00161-X

Walsh JJ, Nicol A, Childs C (2002) An alternative model for the growth of faults. Journal of Structural Geology 24:1669-1675. https://doi.org/10.1016/S0191-8141(01)00165-1

Walsh JJ, Watterson J (1988) Analysis of the relationship between displacements and dimensions of faults. Journal of Structural Geology 10:239-247. https://doi.org/10.1016/0191-8141(88)90057-0

Walsh JJ, Watterson J (1989) Displacement gradients on fault surfaces. Journal of Structural Geology 11:307-316. https://doi.org/10.1016/0191-8141(89)90070-9

Wilkins SJ, Gross MR (2002) Normal fault growth in layered rocks at Split Mountain, Utah: Influence of mechanical stratigraphy on dip linkage, fault restriction and fault scaling. Journal of Structural Geology 24:1413-1429. https://doi.org/10.1016/S0191-8141(01)00154-7

Willemse EJM, Pollard DD, Aydin A (1996) Three-dimensional analyses of slip distributions on normal fault arrays with consequences for fault scaling. Journal of Structural Geology 18:295-309. https://doi.org/10.1016/S0191-8141(96)80051-4

Yielding G, Freeman B, Needham DT (1997) Quantitative fault seal prediction. AAPG Bulletin 81:897-917. https://doi.org/10.1306/522B498D-1727-11D7-8645000102C1865D